Journal of The Electrochemical Society, **150** (11) B512-B516 (2003)
0013-4651/2003/150(11)/B512/5/$7.00 © The Electrochemical Society, Inc.

Cerium Deposition on Aluminum Alloy 2024-T3 in Acidic NaCl Solutions

A. Kolics,*[,a] A. S. Besing,*[,b] P. Baradlai,[c] and A. Wieckowski*[,z]

Department of Chemistry and Frederick Seitz Materials Research Laboratory, University of Illinois at Urbana-Champaign, Urbana, Illinois, USA

We analyzed the interaction of cerium ions with surface intermetallics on Al 2024-T3 in NaCl media under open circuit conditions at pH 3 using scanning electron microscopic, Auger-electron spectroscopic (AES), and energy dispersive X-ray techniques (EDX), as well as electrochemistry. The results indicate that cerium deposition in a pH 3.0 NaCl solution is strongly surface-site specific. The cerium deposition was the highest on the S-phase particles, lower on the $(Cu,Fe,Mn)Al_6$ sites, and minimal on the bulk matrix. In addition to the formation of a cerium-rich film on the intermetallics, we found that cerium incorporated into the porous structure of the dealloyed S-phase particles (Cu-Mg-Al intermetallics). Our analyses show that cerium does not prevent the dealloying of the intermetallic particles; in fact, the dealloying is necessary for local cerium deposition. AES and EDX data also revealed significant chloride enrichment on the cerium-rich sites. From our electrochemical measurements we conclude that the cerium-rich layer formed in acidic solution at short exposure times does not inhibit cathodic reaction on the intermetallics.

Manuscript submitted August 8, 2002; revised manuscript received February 20, 2003. Available electronically September 22, 2003.

There is an increasing need to find alternatives for chromate in corrosion protection procedures involving 2000 series aluminum alloys.[1] Cerium additives appear to be promising candidates for such a replacement.[1-4] Therefore, the precise inhibition mechanism of cerium needs to be identified. Apparently, in copper containing aluminum alloys, especially Al 2024, cerium(III) acts as a cathodic inhibitor by forming a cerium rich layer on the cathodic sites, hence blocking the electrochemical reactions.[2-4] Using energy dispersive X-ray analysis (EDX), Davenport *et al.*[2] reported that cerium enrichment occurred almost exclusively on the copper-rich intermetallics with no cerium present on the Fe/Mn rich particles. Extended X-ray absorption fine structure (EXAFS) analysis indicated the presence of Ce(IV), especially above pH 8, after a prolonged exposure of Al 2024 alloy to the aerated Ce(III) containing solutions.[3] Nevertheless, Ce(III) enhances the cathodic activity on Al_2Cu phase as reported recently.[5]

While there is a consensus as to the formation of cerium containing layers on the copper-rich intermetallics, it is not known how the stability of intermetallics is affected by cerium ions in a corrosive medium. Previous studies have shown that, in inhibitor-free NaCl solution, the S-phase particle (Cu-Mg-Al intermetallics) undergoes extensive dealloying through the preferential dissolution of aluminum and magnesium.[6-11] The dealloying in acidic solutions also results in major morphological changes. Specifically, most of the S-phase particles exhibit a porous structure[7,8,10] and are often surrounded by a groove, indicating extensive dissolution of the immediately neighboring matrix. This transformation creates highly reactive local cathodic sites on the surface.[6-13] The other most common phase, the $(Cu,Fe,Mn)Al_6$ intermetallic, also enriches in copper, especially in acidic solution, while it develops a thick iron oxide corrosion product layer in near neutral media.[10-11] The bulk matrix also undergoes dealloying and develops a rough surface structure in both acidic and alkaline solutions.[10,12]

Recently, it was shown that the presence of chromate ions can significantly inhibit the dealloying of S-phase particles and the corrosion of Fe-rich intermetallics.[10] Because the intermetallics play a critical role in the corrosion susceptibility of the alloy, it is of special interest to see not only how the intermetallics affect cerium deposition but also how cerium influences the localized reaction, *i.e.*, the dealloying of the particles.

Responding to these issues experimentally, we used a combination of microscopic and spectroscopic techniques, such as Auger-electron spectroscopy (AES), scanning electron microscopy (SEM), and EDX. Additional information on the Al 2024-cerium interaction is also furnished by electrochemistry. The cerium-intermetallic interactions are highlighted through the analysis of the deposition behavior of cerium in acidic solutions, specifically at pH 3.0, as such pH usually develops during localized corrosion.[14] Under such conditions Ce(III) has less tendency to hydrolyze and oxidize to some sparingly soluble Ce(IV) compounds.[15]

Experimental

Samples were made of Al 2024-T3 alloy of $0.6\ cm^2$ geometric surface area. Prior to the experiments, the samples were wet polished with SiC emery paper down to no. 2400 followed by a polishing down to no. 4000 using glycol lubricant. After polishing, the samples were ultrasonicated in isopropyl alcohol for 10 min and washed briefly with Millipore water before introduction to the measuring cell for electrochemical characterization. The $Ag/AgCl([Cl^-] = 3\ M)$ half-cell and a platinum gauze were used as reference and counter electrodes, respectively. All potentials quoted in this paper are given *vs.* the Ag/AgCl reference, which is 0.20 V negative to the standard hydrogen electrode (SHE). Prior to chronoamperometric analysis, the electrode was held at open circuit potential for 45 min in cerium containing or cerium-free sodium chloride solution. After 45 min, the electrode potential was changed to a value more negative than the open circuit potential (OCP) and the current was measured as a function of time. The supporting electrolyte was 0.1 M NaCl solution, pH 3.0, with the solution pH adjusted to 3.0 by HCl addition. All solutions were prepared from analytical reagent grade quality chemicals using Millipore water.

Ultrahigh vacuum (UHV) measurements were conducted using a Physical Electronic Industries, PHI model 660 AES spectrometer. In AES and scanning Auger microscopic (SAM) studies, a 10 kV electron beam energy with an emission current of 40 nA was applied. The samples used in the UHV program were pretreated in the same manner as those in electrochemical experiments except that polishing was continued down to 1 μm with diamond slurry in glycol lubricant in order to minimize the effect of surface roughness in the spectroscopic analysis. Further experimental steps were the same as discussed previously.[10]

Sample imaging by SEM and the EDX analyses were performed using a Hitachi S-4700 microscope equipped with a field emission electron gun. The accelerator voltage for imaging was set to 10 kV, while 20 kV was used for quantitative analysis. The sample was not tilted for imaging or qualitative/quantitative analyses. In some cases,

---

* Electrochemical Society Active Member.
[a] Present address: Blue29 Corporation, Sunnyvale, CA 94089.
[b] Present address: United Technologies Research Center, East Hartford, CT 06108.
[c] On leave from: Department of Radiochemistry, University of Veszprém, Veszprém, H-8201 Hungary.
[z] E-mail: andrzej@scs.uiuc.edu

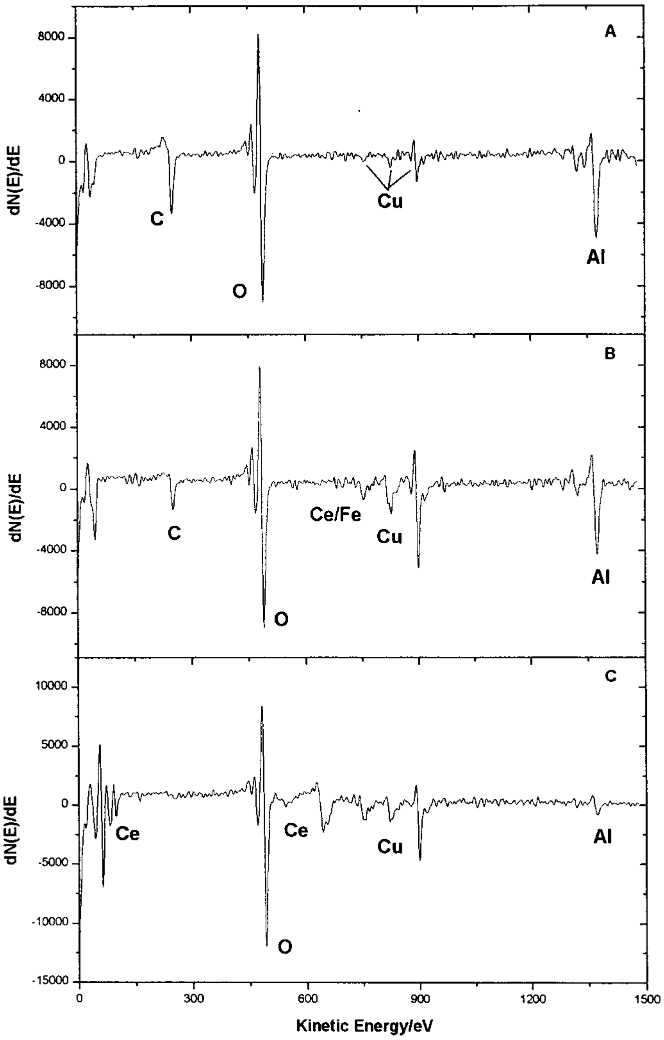

Figure 1. AES analysis of features on Al2024-T3 alloy exposed to 0.1 M NaCl + 10 mM $CeCl_3$, pH 3.0 solution for 45 min. (A) bulk matrix, (B) $(CuFeMn)Al_6$ intermetallics, and (C) S-phase particles.

to avoid possible charging effects, a thin Au-Pd layer was deposited on the sample before analysis.

Special care was taken for the EDX analyses, especially at the S-phase particles, since the EDX sampling volume is usually larger than the size of the particle. In such cases, the bulk matrix contribution to the spectrum cannot be neglected. This contribution is, however, strongly dependent on the size of the particle, which cannot be judged by simple SEM analysis. Therefore, EDX analyses were performed on the same surface sites before and after exposure to aqueous solutions. This was achieved by making reference marks on the surface to easily locate the same surface site after solution treatment.

Results and Discussion

AES analyses were performed on Al 2024-T3 substrates exposed to 0.1 M NaCl + 10 mM $CeCl_3$, pH 3.0 solution for 45 or 90 min. The bulk matrix exhibited no major compositional change after 45 min of exposure (Fig. 1A); however, 90 min of exposure resulted in a copper enrichment on the surface (Fig. 2A). These data imply that cerium deposition is not instantaneous on the surface in acidic solution and is, therefore, likely to be connected to the local pH increase induced by the cathodic reactions on the copper-rich areas.

The surface morphology of $(Cu,Mn,Fe)Al_6$ intermetallics was the same in absence and presence of cerium in 0.1 M NaCl, pH 3.0, as revealed by our SEM analysis. Nevertheless, AES analyses indicated significant cerium enrichment (Fig. 1B), especially after 90 min of exposure (Fig. 2B). AES depth profiling data evidence a *ca.* 30 nm thick Ce-rich layer and a 150 nm thick oxide layer on the intermetallics (Fig. 3). As seen from the depth profiling results, cerium was enriched only in the top layers of the oxide film. As a comparison, we note that the oxide film thickness on the same type of intermetallic was only *ca.* 15 nm thick after 45 min exposure of the substrate to 0.1 M NaCl + 10 mM Na_2CrO_4, pH 3.0 solution.[10] It is also noteworthy that cerium did not change the relative ratio of the alloying elements in the surface oxide film. Specifically, the Al:Cu:Fe ratio was the same in 0.1 M NaCl and 0.1 M NaCl + 10 mM $CeCl_3$ solutions. Comparing these data with our depth profiling results performed on unexposed $(Cu,Fe,Mn)Al_6$ (Fig. 4), we concluded that, unlike chromate,[10] cerium does not inhibit the surface dealloying of the $(Cu,Fe,Mn)Al_6$ intermetallics and, consequently, the surface enrichment of copper. Note that the dealloying of $(Cu,Fe,Mn)Al_6$ intermetallics is significantly lower than that of S-phase particles; therefore, the porosity of the Cu-Mg-Al intermetallics will be considerably higher.[10,11] This is in line with our AES observation because notable incorporation of cerium deep into the $(Cu,Fe,Mn)Al_6$ intermetallic structure was not found.

The most significant cerium deposition was detected on the $CuMgAl_2$ intermetallics (Fig. 1C and 2C). The AES depth profiling analyses performed on S-phase particles show significant amounts of oxygen and cerium even at a depth of 1 μm (Fig. 5). The particle was also enriched in copper in the entire analysis depth and shows

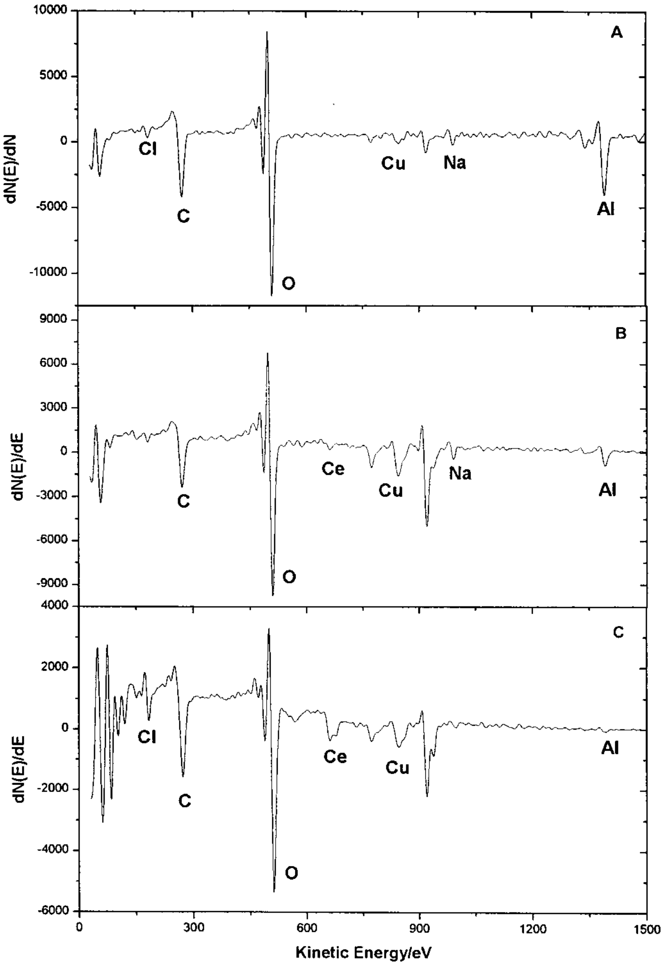

Figure 2. AES analysis of features on Al2024-T3 alloy exposed to 0.1 M NaCl + 10 mM $CeCl_3$, pH 3.0 solution for 90 min. (A) bulk matrix, (B) $(CuFeMn)Al_6$ intermetallics, and (C) S-phase particles.

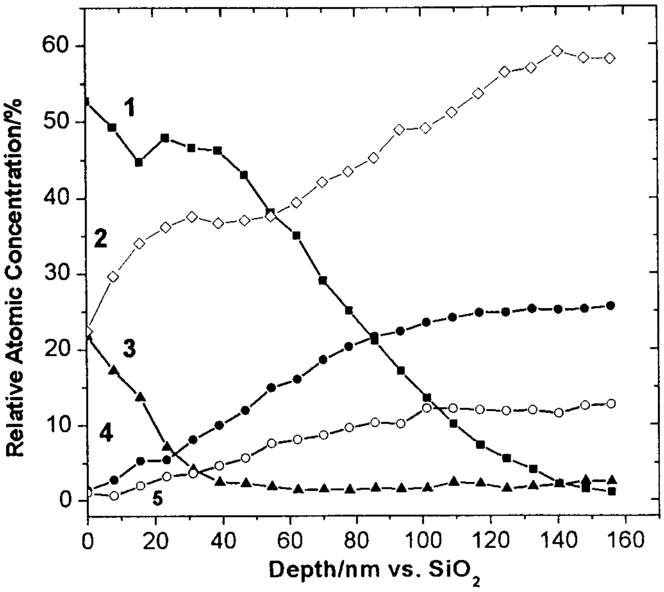

Figure 3. AES depth profiling analysis of $(CuFeMn)Al_6$ intermetallic after 90 min exposure of Al 2024-T3 substrate to 0.1 M NaCl + 10 mM $CeCl_3$, pH 3.0 solution. (1) oxygen, (2) aluminum, (3) cerium, (4) copper, (5) iron.

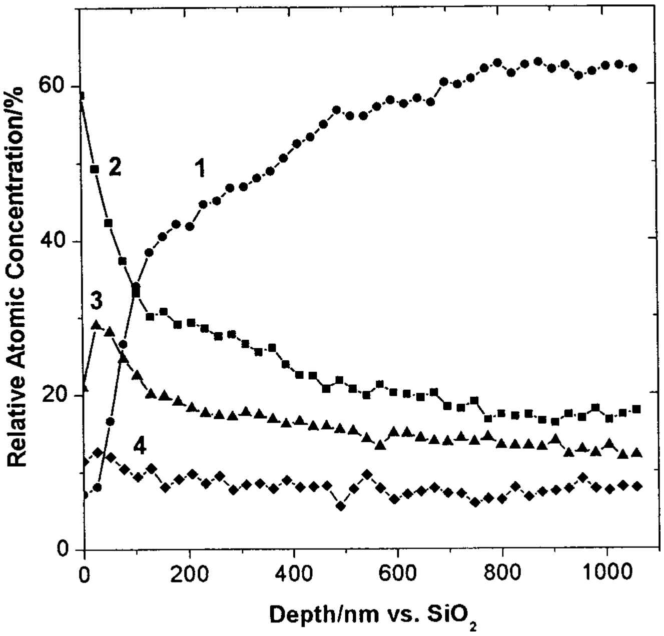

Figure 5. AES depth profiling analysis of S-phase particles after 90 min exposure of Al 2024-T3 substrate to 0.1 M NaCl + 10 mM $CeCl_3$, pH 3.0 solution. (1) copper, (2) oxygen, (3) cerium, (4) aluminum.

no sign of magnesium, which is indicative of extensive dealloying. These results are also in line with the present (Fig. 6) and previous EDX analyses.[10] Namely, S-phase particle exhibited a strong magnesium peak in the EDX spectrum before solution exposure,[10] while the same particles exposed to acidic NaCl solutions showed little or no magnesium in the particle. SEM imaging provided further evidence on the inability of cerium to prevent dealloying (Fig. 7). Namely, the S-phase particles exhibited a porous structure similar to that observed in the absence of cerium. Therefore, it is likely that cerium detected within the intermetallics was due to cerium deposition within the pores of the particle. Imaging analysis by SEM as well as elemental mapping by Auger indicated that, typically, the cerium deposit did not cover the entire particle.

Another interesting feature of cerium deposition was its chloride deposition enhancing effect. Specifically, the relative concentration of chloride is 0.3 ± 0.1%, 0.8 ± 0.2%, and 1.3 ± 0.5% on the bulk matrix, $(Cu,Fe,Mn)Al_6$ intermetallics and S-phase particles, respectively (Fig. 8A-C). These data imply a possible connection between cerium and chloride deposition. Although such coupled surface accumulation was found earlier,[2,4] no attention was given to this relationship before. We attributed the high chloride content of the deposit to the formation of a sparingly soluble $Ce(OH)_xCl_{3-x}$ compound (where $x = 2.33$ and $\log K_s = -17.7$[16]), which deposited together with $Al(OH)_3$ and $Ce(OH)_3$. The cerium compounds started to deposit at around the same pH, *i.e.*, pH 7.7, under the given concentrations of cerium and chloride ions in the solution. Such a coupled deposition was even more evident when the local cathodic reactions are further enhanced, *i.e.*, by cathodic polarization (see the section on Electrochemical data, below). EDX analysis of an S-phase particle after cathodic polarization indicated enhanced chloride and cerium concentrations (Fig. 9) as compared to that observed after exposure under open circuit conditions (Fig. 6). With cathodic polarization, the cathodic reaction was accelerated, induc-

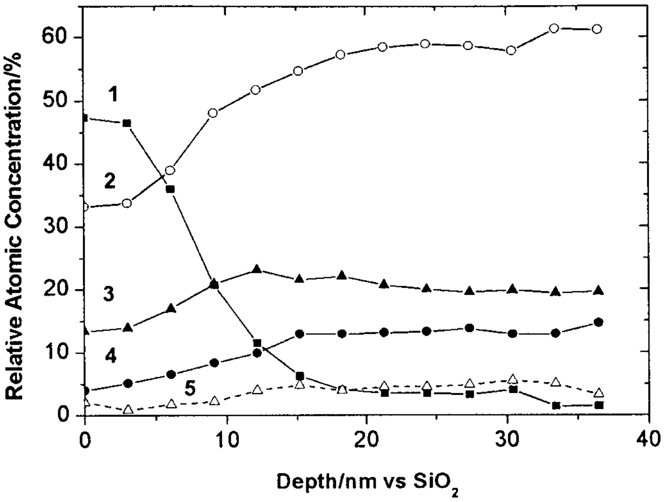

Figure 4. AES depth profiling analysis of $(CuFeMn)Al_6$ intermetallic on Al 2024-T3 after polishing. (1) oxygen, (2) aluminum, (3) copper, (4) iron, (5) manganese.

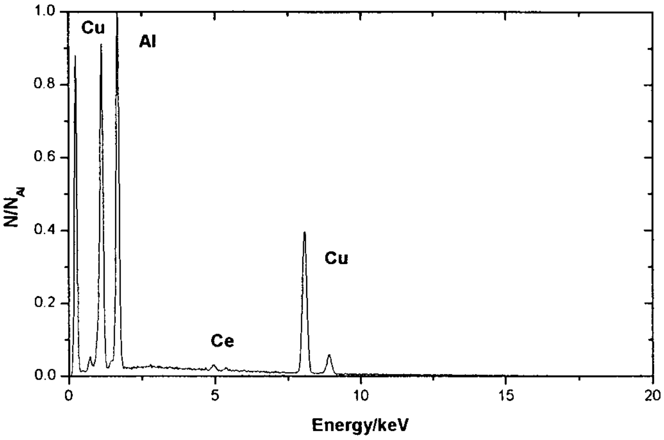

Figure 6. EDX analysis of an S-phase particle on Al2024-T3 alloy exposed to 0.1 M NaCl + 10 mM $CeCl_3$, pH 3.0 solution for 90 min.

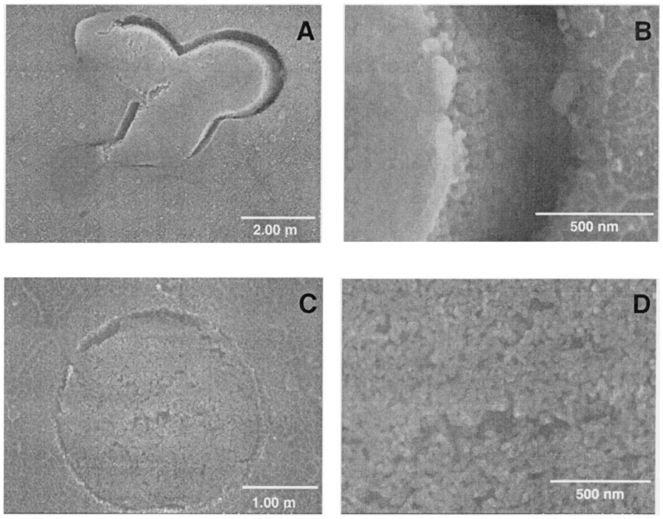

Figure 7. SEM images of S-phase particles on Al2024-T3 alloy after exposing the substrate to 0.1 M NaCl + 10 mM $CeCl_3$, pH 3.0 solution for 90 min. (Images B and D are higher magnification SEM micrographs of particles in image A and C, respectively.)

ing a more pronounced pH increase and, consequently, a higher extent of cerium hydroxide or cerium-hydroxo-chloride deposition.

The presented results indicate that cerium deposition actually proceeded on all surface sites, although to varying degrees, even in acidic solution. The increasing amount of surface cerium with exposure time is related to the dealloying rate of the bulk matrix, $(Cu,Fe,Mn)Al_6$ intermetallics, and S-phase particles. Namely, all surface sites became enriched in copper to a certain degree. The transformation was the fastest and most complete on the S-phase particles. The $(Cu,Fe,Mn)Al_6$ intermetallics and the bulk matrix got more dealloyed as aluminum dissolves from the matrix. Therefore, cerium, in contrast to chromate, does not prevent the dealloying of the intermetallics.

In fact, extensive dealloying of the Al2024 surface is a prerequisite for cerium deposition in acidic media. The effect of copper enrichment on cerium deposition was indirect because the primary reason for the surface accumulation of cerium is the increased local pH *vs.* bulk solution pH. The higher local pH developed due to the cathodic reactions, such as hydrogen ion or oxygen reduction, occurring preferentially on the copper-rich sites. This favors the hydrolysis of cerium(III), which later leads to the formation of a cerium oxide/hydroxide film. The first step in the process is preferential dealloying of magnesium and aluminum at S-phase particles. As the dealloying process continued, the relative copper content of the particles increased, changing the originally anodic particle (*vs.* bulk matrix) to cathodic. The cathodic reactions, which proceeded after extensive dealloying, induced the local pH increase and the hydrolysis of solvated cerium ions.

Judging from the relative atomic concentration of cerium on the surface and the thickness of the cerium-rich layer, the extent of cerium deposition increased in the following order: bulk matrix $< (Cu,Fe,Mn)Al_6$ intermetallics $<$ S-phase particle. However, we note that the relative atomic concentration of cerium varied significantly, *i.e.*, from 0 to 6% on the $(Cu,Fe,Mn)Al_6$ intermetallics and 0 to 22% on the S-phase particles after 45 min exposure. The large spread in the concentration indicates that the electrochemical activity, such as the rate of hydrogen ion reduction, differed markedly even at intermetallics of the same kind. This is in contrast to our findings reported with chromate, because the total chromium, *i.e.*, $Cr(III) + Cr(VI)$, concentration varied only by $\pm 1.5\%$.

Electrochemical data.—We measured the OCP change *vs.* time in the absence and presence of cerium(III) ions in 0.1 M NaCl solution. These results indicate that there is no substantial difference in the OCP change in the two solutions during the first 90 min. The OCP after 90 min was -0.89 ± 0.06 V and -0.96 ± 0.06 V in the absence and presence of 10 mM $CeCl_3$, respectively. Specifically, the electrode potential did not shift more negative in the presence of cerium, which would indicate the inhibition of cathodic reactions.

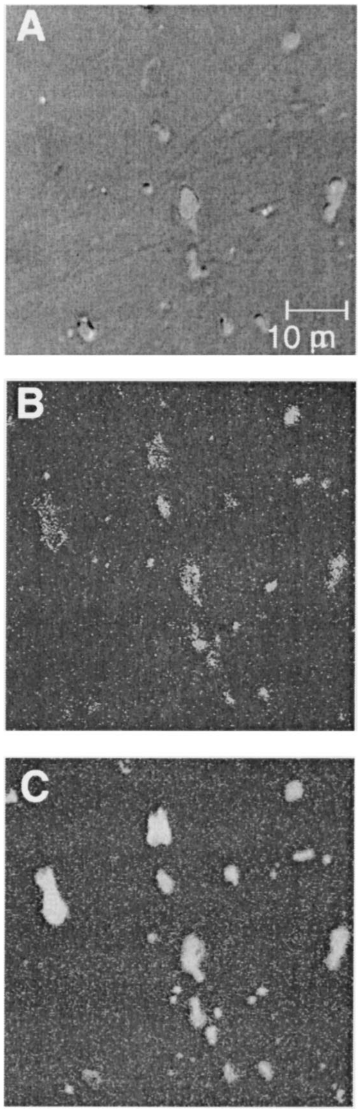

Figure 8. (A) SEM and AES (B) Ce, (C) Cl elemental map from the surface of Al2024-T3 alloy after exposing the substrate to 0.1 M NaCl + 10 mM $CeCl_3$, pH 3.0 solution for 90 min.

Therefore, we suggest that the cerium-rich film formed on the surface does not provide a sufficient barrier layer to block electrochemical processes. This hypothesis is further supported by cathodic chronoamperometric analysis. In this case, after 45 min of exposure at OCP, we held the electrode potential at -1.2 V, *i.e.*, *ca.* 0.2 more negative than the OCP, and measured the current decay (Fig. 10). In this case, the cerium-containing solution indicated higher cathodic activity. This is maintained at electrode potentials negative to -1.2 V. We note that the observed behavior is in alignment with the electrochemical results of Kendig *et al.*[5] obtained on $CuAl_2$ phase at pH 5.4.

In summary, neither the electrochemical nor the surface analytical results evidenced a corrosion inhibition effect by cerium in

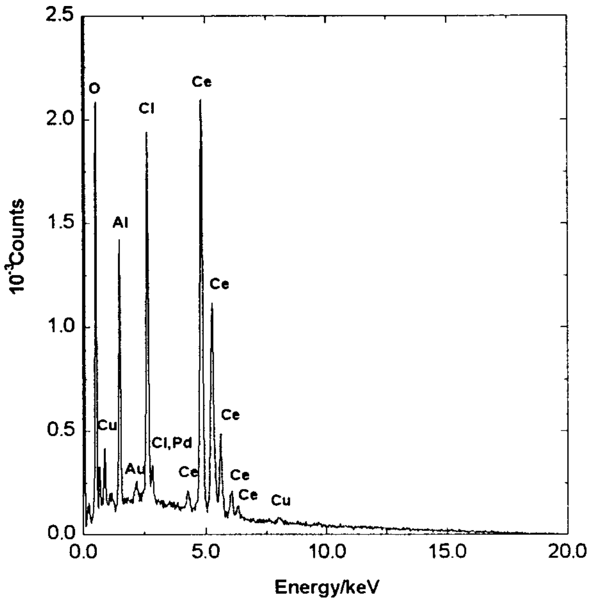

Figure 9. EDX analysis of the deposit formed above the Cu-rich intermetallics on Al2024-T3 alloy in 0.1 M NaCl + 10 mM $CeCl_3$, pH 3.0 at $E = -1.20$ V.

acidic media after short, *i.e.*, 90 min, exposure time. These results are supported by the findings of Hinton *et al.*[17] who reported significant corrosion-inhibiting effects of cerium on other aluminum alloys only after 100 h exposure in near neutral solutions. Based on these assessments, it is likely that a local release of cerium (III) from a cerium-rich coating may not be adequate to prevent a rapidly progressing localized attack because the buildup of a protective film is a slow process, requiring a local pH buildup to initiate cerium deposition.

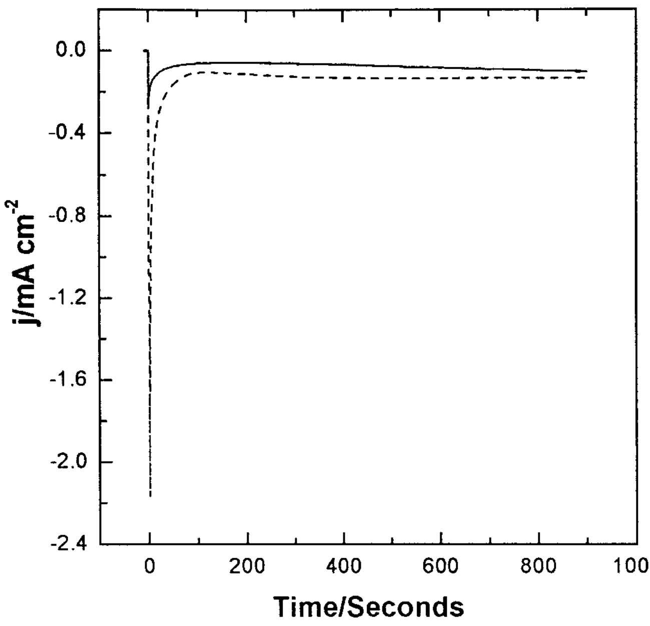

Figure 10. Chronoamperometric analysis of Al2024-T3 alloy at $E = -1.2$ V after its exposure to pH 3.0 solutions of 0.1 M NaCl (——) and 0.1 M NaCl + 10 mM $CeCl_3$ (— — —) for 45 min at OCP.

Conclusions

The accumulation of cerium on Al 2024-T3 was analyzed in acidic NaCl media. Our data indicate that the cerium deposition increased in the order: bulk matrix $<$ (Cu,Fe,Mn)Al_6 intermetallics $<$ dealloyed S-phase particles. We conclude that heterogeneous cerium distribution on the Al 2024-T3 surface was due to an inhomogeneous pH distribution, which is the result of local cathodic reactions. Because the existence or enhancement of cathodic reactions is a result of dealloying, we conclude that cerium does not inhibit the dealloying of intermetallics and the bulk matrix. In fact, at this pH, the dealloying is a prerequisite for the cerium deposition. As a result, the deposition of cerium in acidic solution is not instantaneous.

Our data also implies that cerium penetrated and filled up the porous structure of the dealloyed S-phase particles. The observed codeposition of chloride with cerium was most likely due to the formation of a cerium-hydroxo-chloride precipitate. This precipitate, together with the cerium ions in the solution, failed to exhibit any inhibiting effect on the cathodic reaction at short exposure time in acidic solution.

Acknowledgments

This material is based upon work supported by the U.S. Department of Energy, Division of Materials Sciences under award no. DEFG02-91ER45439, through the Frederick Seitz Materials Research Laboratory at the University of Illinois at Urbana-Champaign. Assistance from Nancy Finnegan (AES) and Vania Petrova (SEM/EDX) from the Frederick Seitz Materials Research Laboratory is acknowledged. AES and SEM/EDX studies were conducted in the Center for Microanalysis of Materials, University of Illinois at Urbana-Champaign, which is partially supported by the U.S. Department of Energy under grant DEFG02-91-ER45439.

The University of Illinois at Urbana-Champaign assisted in meeting the publication costs of this article.

References

1. F. Mansfeld and Y. Wang, *Br. Corros. J., London*, **29**, 194 (1994).
2. A. J. Davenport, H. S. Isaacs, and M. W. Kendig, *J. Electrochem. Soc.*, **136**, 1837 (1989).
3. A. J. Aldykewicz, H. S. Isaacs, and A. J. Davenport, *J. Electrochem. Soc.*, **142**, 3342 (1995).
4. A. E. Hughes, R. J. Taylor, B. R. W. Hinton, and L. Wilson, *Surf. Interface Anal.*, **23**, 540 (1995).
5. M. Kendig, S. Jeanjaquet, R. Addison, J. Waldrop, *Surf. Coat. Technol.*, **140**, 58 (2001).
6. G. S. Chen, M. Gao, R. P. Wei, *Corrosion (Houston)*, **8**, 52 (1996).
7. R. G. Buchheit, R. P. Grant, P. F. Hlava, B. McKenzie, and G. L. Zender, *J. Electrochem. Soc.*, **144**, 2621 (1997).
8. V. Guillaumin and G. Mankowski, *Corros. Sci.*, **41**, 421 (1999).
9. T. Suter and R. C. Alkire, *J. Electrochem. Soc.*, **148**, B36 (2001).
10. A. Kolics, A. S. Besing, and A. Wieckowski, *J. Electrochem. Soc.*, **148**, B322 (2001).
11. G. O. Ilevbare and J. R. Scully, *J. Electrochem. Soc.*, **148**, B196 (2001).
12. A. Kolics, A. S. Besing, T. Suter, H. Böhni, C. H. Paik, R. C. Alkire, and A. Wieckowski, in *Corrosion and Corrosion Prevention of Low Density Metals and Alloys*, B. Shaw, R. Buchheit, and J. P. Moran, Editors, PV 2000-23, p. 10, The Electrochemical Society Proceedings Series, Pennington, NJ (2001).
13. A. Kolics, J. C. Polkinghorne, A. E. Thomas, and A. Wieckowski, *Chem. Mater.*, **10**, 892 (1998).
14. A. Turnbull, *Corros. Sci.*, **23**, 833 (1983).
15. N. E. Topp, *The Chemistry of the Rare-Earth Elements*, p. 56, Elsevier Publishing Company, New York (1965).
16. *Stability Constant of Metal-Ion Complexes*, Section I, Special Pub. no. 17, Compiled by L. G. Sillen, Chemical Society, Burlington House, London, U.K. (1964).
17. B. R. W. Hinton, D. R. Arnott, and N. E. Ryan, *Met. Forum*, **9**, 162 (1986).